Chinese Chemical Letters 35 (2024) 109645

Contents lists available at ScienceDirect

Chinese Chemical Letters

journal homepage: www.elsevier.com/locate/cclet

Cucurbit[8]uril-based non-covalent heterodimer realized NIR cell imaging through topological transformation from nanowire to nanorod

Jianqiu Li, Yi Zhang, Songen Liu, Jie Niu, Rong Zhang, Yong Chen*, Yu Liu*

College of Chemistry, State Key Laboratory of Elemento-Organic Chemistry, Nankai University, Tianjin 300071, China

ARTICLE INFO

Article history:
Received 12 December 2023
Revised 28 January 2024
Accepted 4 February 2024
Available online 10 February 2024

Keywords:
Multivalent assemblies
Cucurbituril
Morphological transformation
Targeted imaging

ABSTRACT

In recent years, multicolor cascade supramolecular assemblies with controllable topological morphology have become a research hotspot due to their wide application in light-emitting materials, cell imaging and other fields. Herein, several kinds of macrocycles including cucurbiturils, calixarene and cyclodextrins are used as building blocks to construct fluorescent assemblies with anthryl-conjugated phenylpyridine (G), wherein cucurbit[8]uril (CB[8]) and G can form nanowires at a stoichiometric ratio of n:n through host-guest encapsulation to form a non-covalent heterodimer. Significantly, the macrocycle confinement effect drastically enhances the fluorescence emission of G and emission peak generated bathochromic shift from 500 nm to 600 nm. When the supramolecular polymer is further assembled with amphiphilic calix[4]arene (SC4A8), the fluorescence emission of G⊂CB[8] further increases to 1.4 times, accompanied by the morphological transformation from linear structure to nanorod structure. Subsequently, a very small amount of dye Cy5 is added to the assembly solution as an energy receptor, and the negatively charged G⊂CB[8]@SC4A8 system is regarded as an energy donor. The efficient energy transfer process enables near-infrared (NIR) emission at 675 nm with 71% energy transfer efficiency (Φ_{ET}) at a donor/receptor ratio of 100:1. Finally, the cascade supramolecular assembly has been successfully applied to targeted imaging in the nucleus of HeLa and A549 cancer cells.

At present, promoting organic chromophore luminescence by cascade supramolecular assemblies has become one of the research hotspots. Particularly, multivalent supramolecular assemblies based on macrocyclic compounds have successfully expanded the application of artificial nanomaterials in the areas of cell imaging [1], hydrogels [2], information security [3,4] and luminescence materials [5–8]. Compared with crystallization [9], doping [10], or polymerization [11], the cascade supramolecular assembly can not only enhance the luminescence performance of the guest but also endow the system with different topological morphology by noncovalent interactions (such as electrostatic interaction [12,13], multiple hydrogen bonds [14,15], host-guest interaction [16]). In general, cascade supramolecular systems consisted of one guest molecule and two kinds of macrocycles. Among the various macrocyles, cucurbituril was widely selected as a first-level macrocyclic building block, which has a large rigid cavity that can well restrict molecular aggregation, rotation and vibration and thus can greatly improve fluorescent or phosphorescent emission or facilitate emission to occur a bathochromic shift [17–19]. For instance, Stoddart and co-workers reported an extended tetracationic cyclophane, which can emit a series of lights from sky blue to yellow by gradually adding CB[8] to an aqueous solution to form the cyclophane binary and ternary ring-in-ring(s) complexes. This work provided a convenient and effective method to achieve tunable multicolor luminescence [20]. Then multiple charged macrocycles such as sulfobutylether-β-cyclodextrin (SBE-β-CD) [21] or SC4AD [22,23] was used as the second-level building blocks, because they can be further assembled with the primary assembly by electrostatic and hydrophobic interactions with positively charged motif, resulting in enhancement of photoluminescence intensity [24]. For example, a dibromophthalimide derivative can generate a weak phosphorescent emission after being encapsulated by cucurbit[7]uril (CB[7]), but the phosphorescence emission intensity was greatly enhanced after further assembling with SC4AD. Finally, a super advanced phosphorescence trapping aggregate was successfully constructed and applied to multicolor cell labelling [25].

In addition, supramolecular assembly can realize multicolor luminescence and other changes in physical and chemical properties through topological morphology transformation [26–30]. We reported a multilevel supramolecular system consisting of

* Corresponding authors.
E-mail addresses: chenyong@nankai.edu.cn (Y. Chen), yuliu@nankai.edu.cn (Y. Liu).

https://doi.org/10.1016/j.cclet.2024.109645
1001-8417/

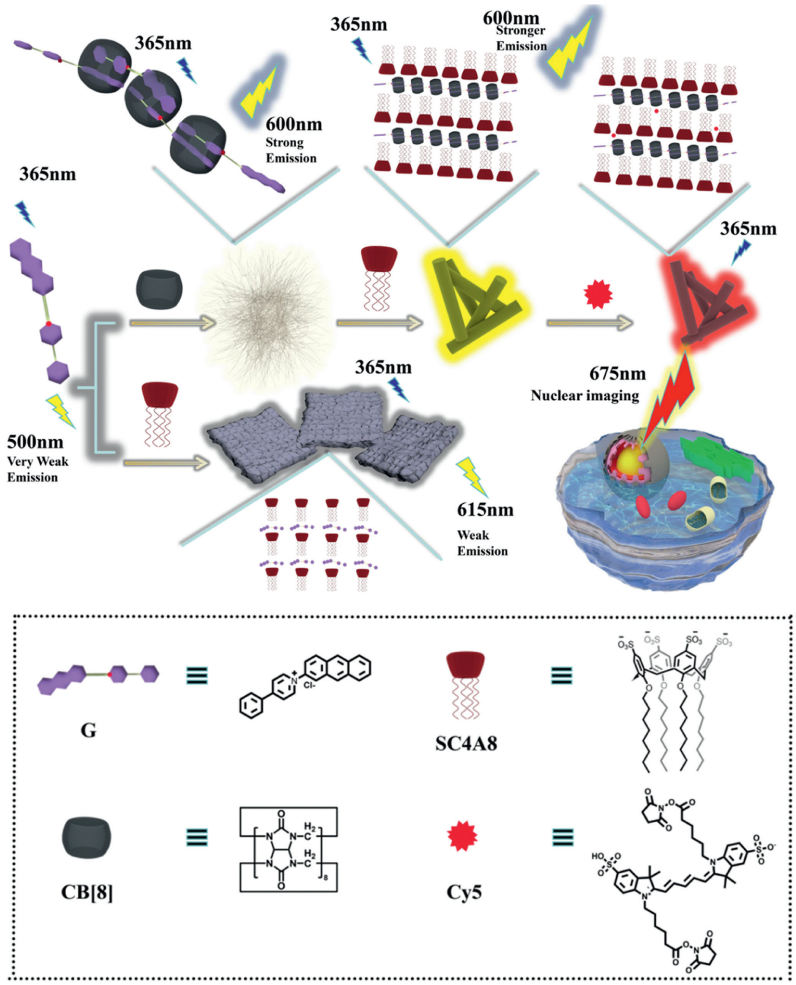

Scheme 1. Schematic illustration of secondary fluorescent energy transfer system.

tetraphenylethylene pyridinium, CB[8] and negatively charged sulfobutylether-β-cyclodextrin, which can achieve multicolor luminescence by regulating topological morphology and was well applied to logic gate systems [31]. However, there were few examples of efficient fluorescence energy transfer with a high donor/acceptor ratio by noncovalent heterodimerization for targeted cell imaging.

Herein, we reported a fluorescence energy transfer system at a donor/receptor ratio of 100:1 based on the multivalent supramolecular assembly. The multivalent supramolecular assembly was constructed from the anthryl-conjugated phenylpyridine (G), CB[8] and amphiphilic SC4A8 by host-guest interaction, electrostatic interaction and hydrophobic interaction (Scheme 1). Firstly, G and CB[8] formed a linear polymer with n:n complexation stoichiometry, and the tight encapsulation greatly enhanced the fluorescence emission of G with bathochromic shift about 100 nm, which had a higher quantum yield than the anthryl-conjugated bromophenylpyridinium salt [32]. Importantly, after the addition of SC4A8, the morphology of the assembly was obviously changed from nanowire to nanorod, accompanied by the further enhancement of fluorescence emission of G⊂CB[8] to 1.4 times. Moreover, the energy acceptor Cy5 was successfully introduced to the G⊂CB[8]@SC4A8 assembly by electrostatic and hydrophobic interactions, thus achieving efficient Förster resonance energy transfer (FRET). Finally, the two-step supramolecular aggregate with NIR emission was also availably employed for targeted imaging in Hela cancer cells and A549 cancer cells. Therefore, this cascade supramolecular assembly with topological transformation and near-infrared emission may provide a simple and efficient method for NIR imaging in cancer cells.

The compound G was synthesized through the Zincke reaction (Scheme S1 and Figs. S1–S6 in Supporting information), and its binding behaviors with CB[8] were explored by UV–vis spectroscopy. As illustrated in Fig. 1a, there were three main absorption peaks of free G at 246, 307 and 345 nm, respectively. As CB[8] gradually increased from 0 to 2.4 equiv., a new absorption peak appeared at 410–550 nm. Meanwhile, the original absorption peak had the bathochromic shift of maximum, the intensity decreased, and three isorption points appeared at 256, 272 and 327 nm. Besides, the solution of G had almost no color, while the solution of G⊂CB[8] appeared bright yellow. These observations suggested that in the cavity of CB[8], the electron-rich anthryl group served as the donor and the electron-deficient pyridinium group served as the acceptor, resulting in the stable charge transfer interaction between molecules. In addition, Job plot exhibited that G could be combined with CB[8] in a 1:1 ratio (Fig. 1b) by measuring the UV–vis spectral variations of different proportions of G and CB[8] at 245 nm (Fig. S7 in Supporting information). Subsequently, when the data of absorption peak at 248 nm were selected to fit the association constant (K_a), K_a obtained between G and CB[8] was determined as 0.94×10^6 L/mol in water at 298 K (Fig. 1c), which proved that the G⊂CB[8] complexation had a high stability at the room temperature. The corresponding fitting formula was shown in Fig. S7 (Supporting information). In addition, ^{1}H NMR titration experiments showed that with the concentration of CB[8] contin-

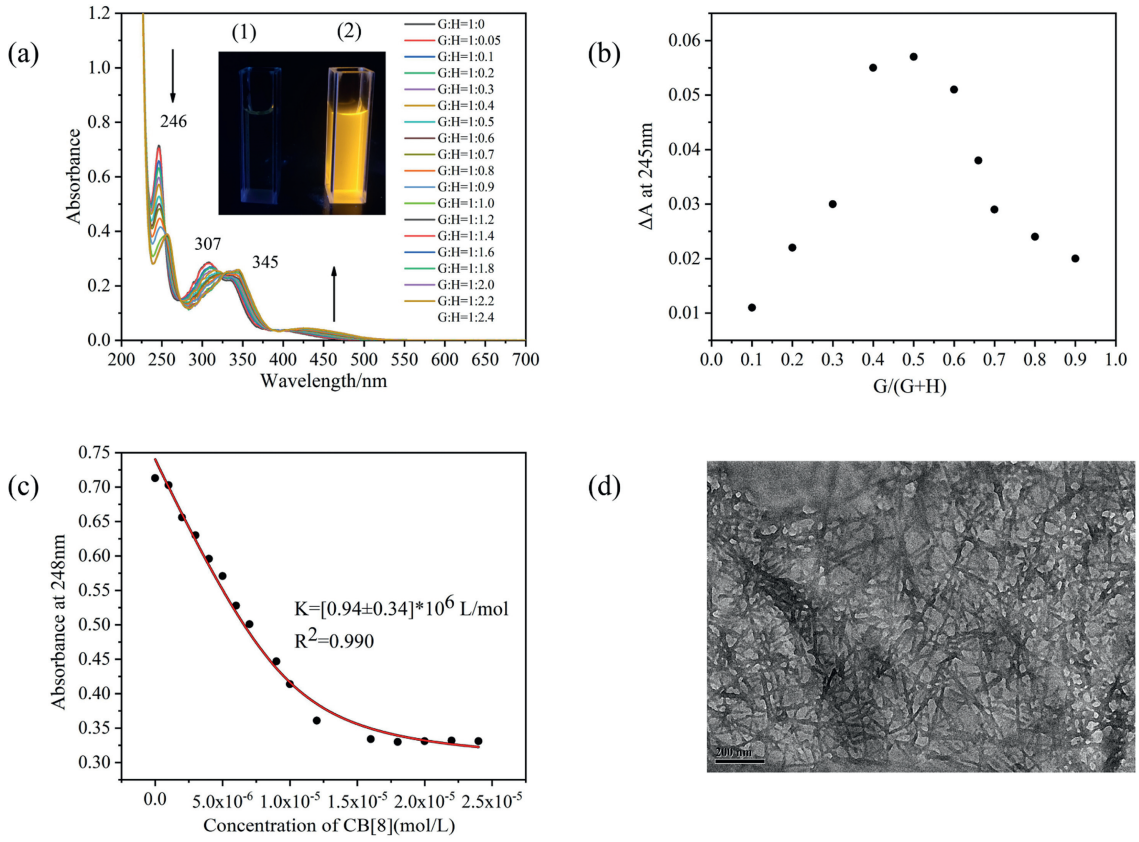

Fig. 1. (a) UV−vis spectral variations of G after adding CB[8] in H_2O. ([G] = 1.0×10^{-5} mol/L and [CB[8]] = 0–2.4×10^{-5} mol/L. Inset: Photographs of G (1) and G⊂CB[8] (2) under ultraviolet lamp. (b) Job plot for G⊂CB[8] complexation in H_2O at 298 K by recording the absorbance at 245 nm. The total concentration is constant ([G] + [CB[8]] = 2.0×10^{-5} mol/L). (c) Absorbance intensity changes of G at 248 nm. (d) TEM image of G⊂CB[8] assembly.

ued to increase, the whole aromatic proton signals of G was broadened and underwent obvious upfield shifts, indicating the formation of large aggregates (Fig. S8 in Supporting information). Subsequently, in the diffusion ordered spectroscopy experiments, the diffusion coefficients (D) of G decreased from 3.03×10^{-10} m^2/s to 1.27×10^{-10} m^2/s after adding in CB[8] and the apparent degree of aggregation was calculated to be 13.6, which further indicated that host and guest formed the large aggregates due to strong inclusion (Figs. S9 and S10 in Supporting information). According to 2D nuclear overhauser effect spectroscopy (Fig. S11 in Supporting information), an obvious correlation signal was generated between anthryl group and pyridinium group, which further proved the dislocation stacking pattern of G in the cavity of CB[8]. Besides, G was more likely to be encapsulated in the cavity of CB[8] in the form of non-covalent heterodimerization and supramolecular polymers were more likely to grow as non-linear chains in a stepped pattern, thus avoiding undesirable steric hindrance between two guest molecules based on previous work reported by our group [32]. Meanwhile, TEM images indicated that many linear nanoaggregates were a length of hundreds of nanometers and an average width of 15 nm. It may be attributed to the further aggregation of several G⊂CB[8] nanowires (Fig. 1d). In addition, DLS data indicated that the measured mean hydrodynamic diameter was 359 nm (Fig. S12 in Supporting information). Therefore, we inferred that the compound of G⊂CB[8] further led to the appearance of supramolecular nanowires.

In order to better explain the non-covalent heterodimerization effect, three kinds of macrocycles, namely sulfato-β-cyclodextrin (SCD), SC4A8 and CB[7] were used as the reference molecules to compare their assembly behaviors to G with that of CB[8]. As shown in Figs. S13-S15 (Supporting information), CB[7] carried out a 1:1 binding mode with G, the K_a between CB[7] and G (1.0×10^6 L/mol) measured by UV−vis spectroscopy was very comparable to K_a in Fig. 1c. Besides, ^{1}H NMR titration experiments showed that after adding CB[7], the proton of the pyridinium (H_a) underwent the downfield shift and the protons of the anthryl ($H_{l,k,i}$) shifted to upfield, which further proved the bonding mode between G and CB[7] (Fig. S16 in Supporting information). In addition, as the concentration of free SC4A8 changed from 10 μmol/L to 100 μmol/L, the optical transmittance at 550 nm was basically consistent, which indicated that the free SC4A8 could not form aggregates in a certain concentration range (Fig. S17 in Supporting information). The critical aggregation concentrations (CAC) of G in the presence of SC4A8 was determined by detecting the change of the optical transmittance at 520 nm under different concentration of G. After adding SC4A8, the transmittance at 520 nm decreased gradually, signaling that a large aggregate was formed in the solution, and an inflection point at 19 μmol/L appeared, which was a complexation-induced CAC value of G in the presence of SC4A8 (Fig. S18 in Supporting information). Moreover, to determine the optimal molar ratio of SC4A8 to G, we monitored the optical transmittance of G by continuously adding SC4A8 to the solution of G with a steady concentration of 50 μmol/L. The transmittance at 520 nm declined promptly and then gradually increased to a *quasi*-plateau, and the minimum was obtained when the concentration of SC4A8 was 11.67 μmol/L (Fig. S19 in Supporting information). In addition, it could be found that G⊂SC4A8 assembly had an obvious Tyndall effect. Similarly, the minimum for G⊂SCD system was measured at a concentration of SCD as 10 μmol/L (Figs. S20 and S21 in Supporting information). Therefore, the preferred mixing ratio of

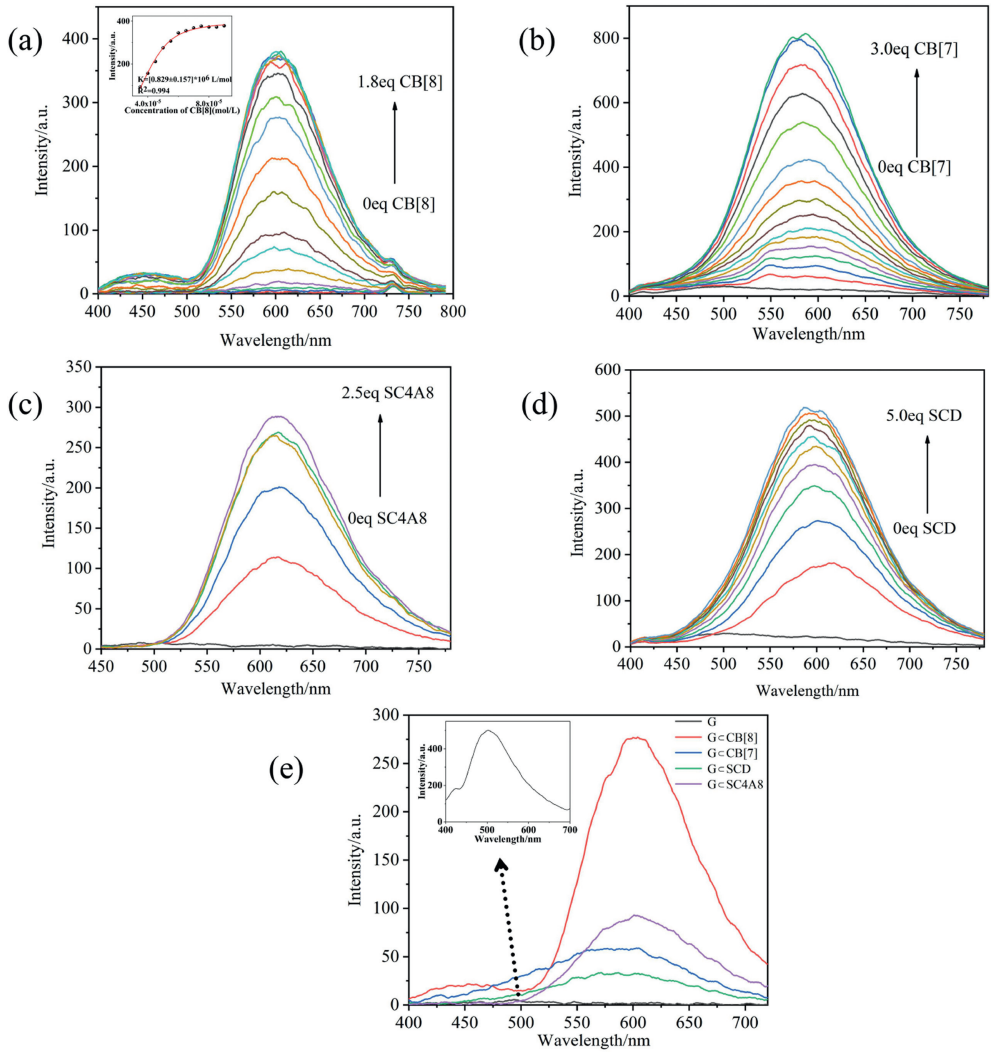

Fig. 2. Fluorescence spectra of free G in the presence of different ratios of (a) CB[8] ($0–9 \times 10^{-5}$ mol/L; slits: 5/5 nm (inset: fluorescence intensity changes of G at 600 nm), (b) CB[7] ($0–15 \times 10^{-5}$ mol/L; slits: 10/10 nm), (c) SC4A8 ($0–12.5 \times 10^{-5}$ mol/L; slits: 10/5 nm), and (d) SCD ($0–25 \times 10^{-5}$ mol/L; slits: 10/10 nm) in H_2O at 298 K ($[G] = 5.0 \times 10^{-5}$ mol/L). (e) Fluorescence contrast analysis of G, G⊂CB[8], G⊂CB[7], G⊂SC4A8, G⊂SCD ($(G) = (CB[8]) = 5 \times 10^{-5}$ mol/L; slits: 5/5 nm (inset: Fluorescence emission of G; slits: 20/20 nm).

the supramolecular aggregate was SC4A8:G = 1:4.3 or SCD:G = 1:5, respectively.

Subsequently, the fluorescence behaviors between G and four different macrocycles were also studied. Initially, G exhibited a extremely faint fluorescence emission at 500 nm in solution. As the proportion of CB[8] gradually increased in the solution of G, the fluorescence emission at 600 nm was greatly increased with bathochromic shift about 100 nm at a G⊂CB[8] ratio of 1:1 (Fig. 2a). In addition, the fluorescence lifetime extended from 3.48 ns to 7.30 ns (Fig. S22 in Supporting information). Meanwhile, K_a of G⊂CB[8] complexation was determined as 0.83×10^6 L/mol, which brought into correspondence with the K_a determined by UV−vis spectroscopy. Similarly, the fluorescence intensity was enhanced in different degrees in G⊂CB[7], G⊂SC4A8, and G⊂SCD systems (Figs. 2b-d). After the addition of CB[7], the fluorescence intensity of G at 585 nm was greatly enhanced with a slight blue shift compared with G⊂CB[8]. This phenomenon may be due to the fact that anthryl and pyridinium were not simultaneously attached to the cavity of CB[7], resulting in non-covalent heterodimerization could not occur. Compared with SCD, the addition of SC4A8 caused a slight bathochromic shift, which could be attributed to the stronger electrostatic interaction between positively charged G and negatively charged SC4A8. In order to highlight excellent fluorescence enhancement effect of CB[8], we compared the fluorescence spectra of G, G⊂CB[8], G⊂CB[7], G⊂SC4A8 and G⊂SCD at the slit of 5/5 nm (Fig. 2e). Initially, G produced a weak fluorescence emission at 500 nm when the slits were enlarged to 20/20 nm (Fig. 2e, inset). Whereafter, compared with the other three macrocycles, G⊂CB[8] could greatly improve the fluorescence intensity of G. A possible reason was that the formation of aggregates promoted the occurrence of charge transfer from electron-rich anthryl group to electron-deficient pyridinium group in the tight cavity of CB[8], thus greatly enhancing the fluorescence of G. In addition, the fluorescence intensity of the G⊂SC4A8 was also higher than that of G⊂CB[7] and G⊂SCD. Finally, the topological morphology of G, G⊂CB[7], G⊂SCD and G⊂SC4A8 were measured by TEM. The images of free G, G⊂CB[7] and G⊂SCD all showed the irregular morphology. While, G⊂SC4A8 formed thick nanosheets of varying sizes due to aggregation between G and SC4A8 by electrostatic interactions (Fig. S23 in Supporting information). Therefore, in order to further enhance the fluorescence intensity of G⊂CB[8], SC4A8 was introduced as the secondary macrocycle because the negatively charged sulfonates could interact with the exposed protons of G by electrostatic interactions.

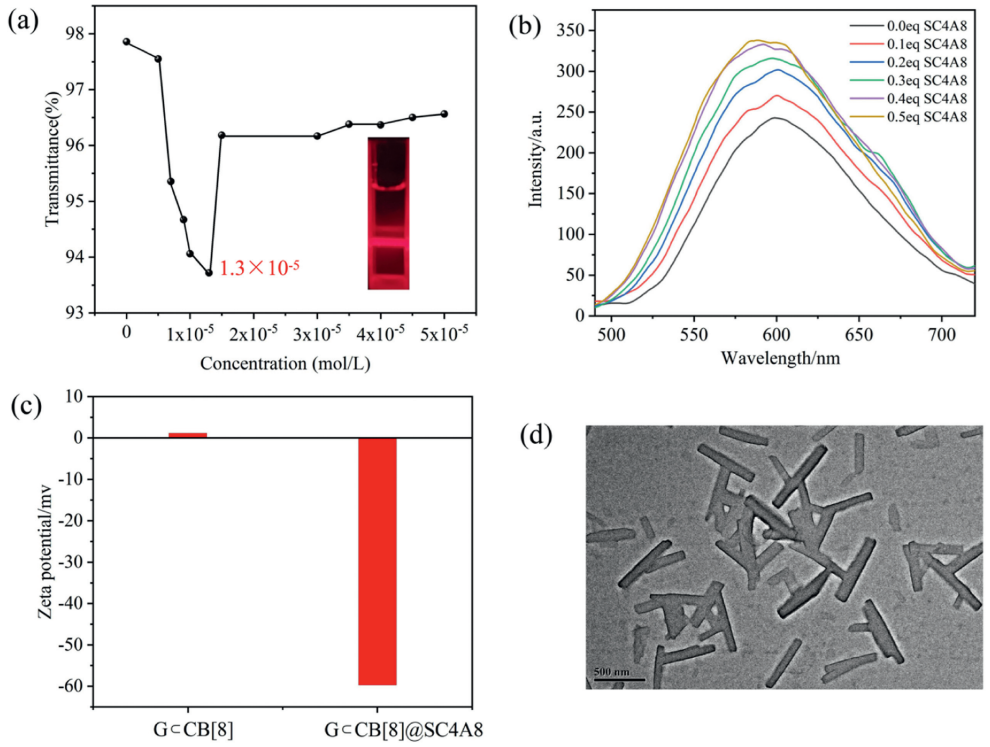

Fig. 3. (a) The correlation between the transmittance at 532 nm and the increase of SC4A8 concentration (inset: Tyndall effect of G⊂CB[8]@SC4A8). (b) Fluorescence spectra of G⊂CB[8] at SC4A8 concentrations ranging from 0 to 0.5 equiv. (c) Zeta potential variation of the assembly after adding SC4A8. (d) TEM image of G⊂CB[8]@SC4A8.

Owing to its octanyl-modified upper portals and sulfonate-laced lower portalsthe [23], strategy of constructing multivalent assemblies by introducing SC4A8 with amphiphilic structure has become an important means to improve the optical properties. SC4A8 can perform secondary assembly with the exposed cationic guest *via* electrostatic interaction, and the long hydrophobic alkyl chain of SC4A8 can also provide the possibility for loading hydrophobic dyes to achieve NIR fluorescence emission. Therefore, after selecting CB[8] as the first-level macrocyclic building block, SC4A8 was introduced as a second candidate for constructing the emission enhancement system. The CAC between G⊂CB[8] and SC4A8 was measured. With the gradual addition of SC4A8 to the solution of G⊂CB[8], the optical transmittance at 532 nm declined rapidly and then recovered gradually with an inflection point appearing when the concentration of SC4A8 reached 13 μmol/L at a fixed concentration of G⊂CB[8] (50 μmol/L). In addition, distinct Tyndall effect could also be observed, which was a good demonstration of lager assemblies formation. The distinct drop of the transmittance before the minimum indicated that SC4A8 and G⊂CB[8] have undergone significant aggregation. When the concentration of SC4A8 was increased to excess, the transmittance increased significantly due to the dissociation of the lager assemblies (Fig. 3a). Therefore, according to the results of CAC experimental results, the optimal ratio of the largest assemblies formed by G⊂CB[8] and SC4A8 was 3.8:1. As depicted in Fig. 3b, the initial fluorescence intensity of G⊂CB[8] progressively increased with the proportion of SC4A8 increasing and reached a maximum of fluorescence intensity when increasing the amount of SC4A8 to 25 μmol/L. During this period, the original fluorescence intensity of G⊂CB[8] improved 1.4 times, and the fluorescence lifetime extended from 7.30 ns to 9.17 ns (Fig. S22 in Supporting information). Furthermore, in comparison to G⊂CB[8], the fluorescence quantum yield of secondary assembly has increased by approximately 2.5 times from 3.24% to 8.04% (Fig. S24 in Supporting information). Subsequently, TEM, zeta potential and DLS experiments were conducted to investigate the co-assembly behavior between G⊂CB[8] and SC4A8. The aggregate gave a negative surface potential value (−59.71 mV, Fig. 3c), indicating that anionic SC4A8 was distributed on the surface of G⊂CB[8]. In addition, TEM image showed many nanorod-like structures with lengths from 220 nm to 820 nm and diameters from 70 nm to 100 nm (Fig. 3d). Moreover, DLS results (Fig. S25 in Supporting information) gave an average particle size of the aggregate as 447 nm. These experimental results demonstrated that the secondary assembly based on SC4A8 not only changed the morphology and potential of supramolecular systems, but also improved the optical properties of G⊂CB[8].

Due to the long hydrophobic alkyl chains of G⊂CB[8]@SC4A8 as well as its bright yellow emission at 600 nm, hydrophobic dye molecules could be loaded for constructing FRET systems. In order to obtain NIR fluorescence emission, Cy5 was chosen as the energy acceptor owing to overlapping significantly with the fluorescence emission peak of energy donor (Fig. 4a). As depicted in Fig. 4b, during the process of adding Cy5 to multivalent supramolecular assemblies, the initial fluorescence peak gradually reduced. At the same time, a new red fluorescence peak appeared at 675 nm when the excitation wavelength was 365 nm. The process of spectral changes could effectively demonstrate the occurrence of energy transfer processes. Intriguingly, the fluorescence intensity of G⊂CB[8]@SC4A8:Cy5 was higher than that of free Cy5 (Fig. S26 in Supporting information), indicated that Cy5 accepted the energy from G⊂CB[8]@SC4A8 and thus emitted the red luminescence emission at 675 nm. In addition, a gradual bathochromic shift in color coordinates was observed in the CIE chromaticity diagram (Fig. 4c). Furthermore, in the G⊂CB[8]@SC4A8:Cy5 conjugate, the Φ_{ET} was up to 71% (Fig. S27 in Supporting information). For comparison, we constructed a FRET system between G⊂SC4A8 and Cy5. Compared to G⊂CB[8]@SC4A8, the Φ_{ET} from G⊂SC4A8 to Cy5 was only 41% and the ratio of donor to receptor was 10:1, much less than 100:1 (Fig. 4d). The reason for the better energy transfer property of G⊂CB[8]@SC4A8 may be that CB[8] can effectively en-

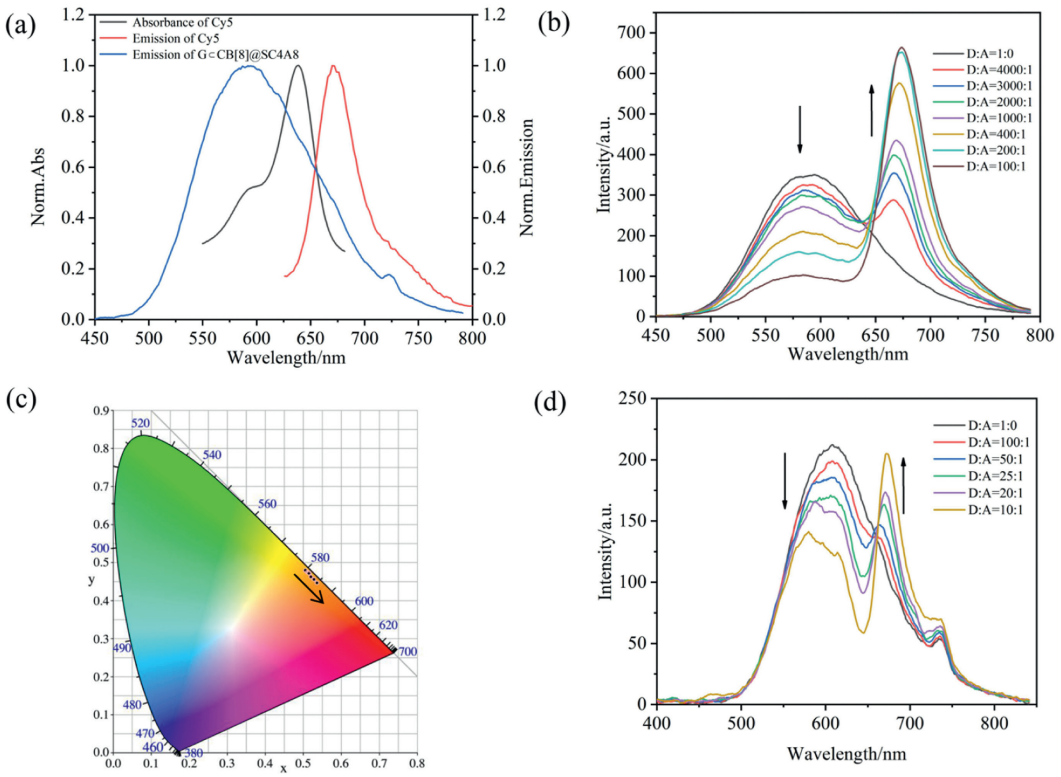

Fig. 4. (a) Normalized emission spectrum of G⊂CB[8]@SC4A8 as well as Cy5, and absorption spectrum of Cy5. (b) Fluorescence emission spectra of G⊂CB[8]@SC4A8 with different proportions of dye Cy5 ([G] = 5.0×10^{-5} mol/L, [CB[8]] = 5.0×10^{-5} mol/L, [SC4A8] = 2.5×10^{-5} mol/L, λ_{ex} = 365 nm). (c) The CIE chromaticity diagram of G⊂CB[8]@SC4A8 containing different ratio of Cy5. (d) Fluorescence emission spectra of G⊂SC4A8 with different proportions of dye Cy5 ([G] = 5.0×10^{-5} mol/L, [SC4A8] = 5.0×10^{-5} mol/L, λ_{ex} = 365 nm).

capsulate G, prevent G from self-stacking and thus avoid the occurrence of ACQ effect, which effectively enhances the fluorescence emission of G. Therefore, under the same excitation conditions, compared with G⊂SC4A8, more energy from G⊂CB[8]@SC4A8 can be transferred to Cy5, resulting in the better energy transfer effect. In addition, the NMR spectra (Fig. S28 in Supporting information) showed that compared with that of free Cy5, there were no significant chemical shift changes in the aromatic region of Cy5 in the Cy5/SC4A8 spectra, while there was a significant chemical shift change in the alkyl chain protons. The displacement of protons in the aromatic region and in the hydrophobic alkyl chain in the ^{1}H NMR Cy5/SC4A8 spectrum indicated that Cy5 was not enclosed in the cavity of SC4A8, but loaded into the hydrophobic chain region of SC4A8. Similarly, the UV–vis and fluorescence spectra of Cy5 were almost unchanged when an equal amount of SC4A8 was added, indicating that SC4A8 did not enclose the chromophore moiety of Cy5 (Fig. S29 in Supporting information). Therefore, in the energy transfer system, SC4A8 played the role of loading hydrophobic dyes, while CB[8] can avoid ACQ effect and enhance the luminescence of the donor through inclusion, which jointly showed the superiority of multivalent supramolecular assemblies.

Due to the marvelous NIR emission properties of the multivalent supramolecular assemblies, the targeted imaging of human cervical carcinoma cells (HeLa cells) and human lung adenocarcinoma cells (A549 cells) were attempted to research its possible application. We added G⊂CB[8]@SC4A8:Cy5 into cell culture medium and continued to culture in cell culture dishes for 12 h and the concentration of NIR reagent was 5 μmol/L. Subsequently, we conducted experiments with confocal laser scanning microscopy to research the biocompatibility and localization features of organelles. As illustrated in Fig. 5, the red luminescence could be observed when the system was under the excitation of the 405 nm laser. Remarkably, the red luminous region overlapped well with the blue nuclear localization agent (Hoechst 33342) due to the appearance of purple areas in the merge image and the Pearson colocalization coefficient in HeLa cells and A549 cells reached 0.87 and 0.77 respectively (Figs. S30 and S31 in Supporting information), which demonstrated the specific nucleus-targeting ability of this assembly in nucleus of cancer cell. In addition, the cells were cultured in a medium containing cell counting kit-8 to evaluate the cytotoxicity of multivalent supramolecular assembly. The results of toxicity experiments showed that the cells could maintain a survival rate of 85% at G⊂CB[8]@SC4A8:Cy5 concentrations ranging from 2 μmol/L to 10 μmol/L compared to the blank experiment, which indicated its low toxicity to cancer cells (Fig S32 in Supporting information). In summary, this multivalent supramolecular assembly can be used as an effective low-toxicity labeling imaging agent for cancer cells.

Herein, we resoundingly constructed a multivalent supramolecular assembly with NIR fluorescence emission exhibiting nucleus-targeted imaging abilities. Although G could only produce weak fluorescence at 500 nm, the fluorescence greatly enhanced and generated bathochromic shift after assembling with CB[8] by the noncovalent heterodimerization. Then, SC4A8 further enhanced the fluorescence intensity by 1.4 times with the morphological transformation of the assembly. Importantly, the assembly could be used as an energy donor for efficient energy transfer with the energy acceptor Cy5, and Φ_{ET} was up to 71% with a high donor/receptor ratio, accompanied by a NIR fluorescence emssion at 675 nm. Furthermore, this nanoassembly could be used as an effective nuclear locator for imaging cancer cells. This study both founds an energy transfer system with a corresponding high donor/acceptor ratio, and provides a valid means for targeting imaging in caner cell.

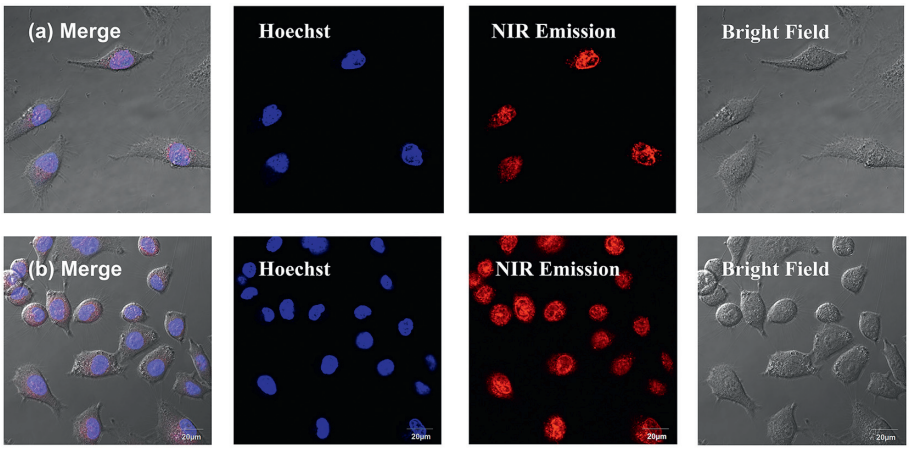

Fig. 5. Cellular imaging of HeLa cancer cells (a) and A549 cancer cells (b) co-stained with G⊂CB[8]@SC4A8:Cy5 for Hoechst 33342, respectively. ([G] = 5.0×10^{-6} mol/L, [CB[8]] = 5.0×10^{-6} mol/L, [SC4A8] = 2.5×10^{-6} mol/L, [Cy5] = 5.0×10^{-8} mol/L). For Hoechst 33342, λ_{ex} = 405 nm, λ_{em} = 420–470 nm. For G⊂CB[8]@SC4A8:Cy5, λ_{ex} = 405 nm, λ_{em} = 650–700 nm.

Declaration of competing interest

The authors declare that they have no known competing financial interests or personal relationships that could have appeared to influence the work reported in this paper.

Acknowledgments

We thank National Natural Science Foundation of China (Nos. 22131008 and 21971127). We also thank the Fundamental Research Funds for the Central Universities and the Haihe Laboratory of Sustainable Chemical Transformations for financial support.

Supplementary materials

Supplementary material associated with this article can be found, in the online version, at doi:10.1016/j.cclet.2024.109645.

References

[1] J.J. Li, H.Y. Zhang, G. Liu, et al., Adv. Opt. Mater. 9 (2021) 2001702.
[2] Y. Zhao, S. Song, X. Ren, et al., Chem. Rev. 122 (2022) 5604.
[3] X. Chen, H.K. Bisoyi, X.F. Chen, et al., Matter 5 (2022) 3883.
[4] Y. Rong, R. Liu, P. Jin, et al., J. Mater. Chem. A 11 (2023) 5895–5901.
[5] P. Xing, C. Yang, Y. Wang, et al., Adv. Funct. Mater. 28 (2018) 1802859.
[6] Y. Sun, L. Jiang, Y. Chen, et al., Chin. Chem. Lett. 35 (2024) 108644.
[7] J. Jiao, G. Sun, J. Zhang, et al., Chem. Eur. J. 27 (2021) 16601–16605.
[8] D. Dai, Z. Li, J. Yang, et al., J. Am. Chem. Soc. 141 (2019) 4756 -476.
[9] O. Bolton, K. Lee, H.J. Kim, et al., Nat. Chem. 3 (2011) 205–210.
[10] Z. Lin, R. Kabe, N. Nishimura, K. Jinnai, C. Adachi, Adv. Mater. 30 (2018) 1803713.
[11] T. Zhang, X. Ma, H. Tian, Chem. Sci. 11 (2020) 482.
[12] Z. Liu, X. Sun, X. Dai, et al., J. Mater. Chem. C 9 (2021) 1958–1965.
[13] Y. Zhang, Z. Xu, T. Jiang, Y. Fu, X. Ma, J. Mater. Chem. C 11 (2023) 1742–1746.
[14] Q. Song, S. Goia, J. Yang, et al., J. Am. Chem. Soc. 143 (2021) 382.
[15] P. Xing, Y. Li, S. Xue, et al., J. Am. Chem. Soc. 141 (2019) 9946–9954.
[16] D.A. Xu, Q.Y. Zhou, X. Dai, et al., Chin. Chem. Lett. 33 (2022) 851–854.
[17] D. Sun, Y. Wu, X. Han, et al., Nat. Commun. 14 (2023) 4190.
[18] X.L. Ni, S. Chen, Y. Yang, Z. Tao, J. Am. Chem. Soc. 138 (2016) 6177–6183.
[19] S.P. Jin, H.L. Wu, L.P. Zhang, et al., Mater. Chem. Front. 7 (2023) 1354–1364.
[20] H. Wu, Y. Wang, L.O. Jones, et al., J. Am. Chem. Soc. 142 (2020) 16849–16860.
[21] P. Zhang, X. Liu, W. Hu, et al., Carbohyd. Polym. 149 (2016) 224–230.
[22] A. Specht, P. Bernard, M. Goeldner, L. Peng, Angew. Chem. Int. Ed. 41 (2002) 4706–4708.
[23] P. Li, Y. Chen, Y. Liu, Chin. Chem. Lett. 30 (2019) 1190–1197.
[24] X.Y. Dai, Y.Y. Hu, Y. Sun, et al., Adv. Sci. 9 (2022) 2200524.
[25] M. Huo, X.Y. Dai, Y. Liu, Angew. Chem. Int. Ed. 60 (2021) 27171–27177.
[26] X.M. Chen, Y. Chen, Q. Yu, et al., Angew. Chem. Int. Ed. 57 (2018) 12519–12523.
[27] H.J. Wang, H.Y. Zhang, W.W. Xing, et al., Chin. Chem. Lett. 33 (2022) 4033–4036.
[28] Y. Li, Y. Dong, X. Miao, et al., Angew. Chem. Int. Ed. 57 (2018) 729–733.
[29] W. Zhang, Y.M. Zhang, S.H. Li, et al., Angew. Chem. Int. Ed. 55 (2016) 11452–11456.
[30] C. Zhang, J. Niu, J. Li, et al., Chin. Chem. Lett. 35 (2024) 108556.
[31] M. Tian, Z. Wang, X. Yuan, et al., Adv. Funct. Mater. 33 (2023) 2300779.
[32] H.J. Yu, Q. Zhou, X. Dai, et al., J. Am. Chem. Soc. 143 (2021) 13887–13894.